

## Robust prestack $Q$ -determination using surface seismic data: Part 1 — Method and synthetic examples

Carl Reine<sup>1</sup>, Roger Clark<sup>2</sup>, and Mirko van der Baan<sup>3</sup>

### ABSTRACT

The accurate determination of seismic attenuation, or  $1/Q$ , is useful for signal enhancement and reservoir characterization. To arrive at the necessary accuracy however, a number of issues must be addressed in the measurement technique. Specifically, spectral interference from closely spaced reflections is a major concern, in addition to the assumptions and errors associated with the raypath geometries of the reference and measured reflections. We have developed a robust method for measuring attenuation from prestack surface seismic gathers that helps minimize these issues. In our prestack  $Q$ -inversion technique; the presence of spectral interference was first reduced by making use of a variable-window time-frequency transform. To minimize the effects of the remaining interference, we then

made use of an inversion scheme operating simultaneously in the frequency and traveltime-difference coordinates. A by-product of this inversion was a collection of the frequency-independent amplitude changes, which in the absence of geometric spreading, contains valuable amplitude variation with angle information, free from attenuation amplitude losses. Furthermore, under the assumption of locally 1D velocity and attenuation distributions, we made use of the  $\tau$ - $p$  transform to operate on traces of constant horizontal slowness. This allowed angle-dependent effects in the overburden such as attenuation anisotropy and source or receiver directivity to be eliminated. In the second part of our study, published separately, this technique was also demonstrated upon a shallow 3D seismic survey, and the measurements compared to another  $Q$ -estimation technique, as well as measurements from a vertical seismic profile.

### INTRODUCTION

As a seismic wave propagates, attenuation, parameterized by  $1/Q$ , typically causes the amplitudes of the higher-frequency components to decay more rapidly than those of the lower frequencies. This effective attenuation is comprised of anelastic losses from absorption, and elastic losses due to scattering, with a combined result that the amplitude of the wave is decreased and the bandwidth and the peak frequency of the data are reduced.

Anelastic, or intrinsic, attenuation is linked to a variety of petrophysical parameters that hold valuable information for reservoir development. Attenuation due to friction between grains or crack faces is controlled by the grain architecture and the effective pressure on the medium (Johnston et al., 1979). Attenuation also occurs as pore fluids move relative to the rock frame, or along cracks as they are compressed (Dvorkin and Nur, 1993). For the fluid case,

the amplitude losses depend on the properties of the fluid, such as viscosity, compressibility, saturation, and on the properties of the pores, including porosity, permeability, and fracture geometry.

Attenuation is typically viewed as a nuisance, because it reduces the overall resolution of seismic data, and makes the interpretation and mapping of geological interfaces more difficult. However, by measuring attenuation, it is possible to make use of it for other geophysical purposes. Inverse  $Q$ -filtering (Wang, 2002) may be incorporated into the processing flow to compensate for the loss of resolution, enabling more reliable structural interpretations (Kaderali et al., 2007). Attenuation-corrected data also allow for the calculation of more accurate angle-dependent reflectivity changes because a significant source of systematic error has been removed (Luh, 1993; Bansal et al., 2009). Additionally, full-waveform inversion can achieve improved accuracy by incorporating attenuation into the initial model (Causse et al., 1999).

Manuscript received by the Editor 18 February 2011; revised manuscript received 12 August 2011; published online 8 February 2012.

<sup>1</sup>Formerly University of Leeds, School of Earth and Environment, Leeds, U. K.; presently Nexen Inc., Calgary, Canada. E-mail: carl\_reine@nexeninc.com.

<sup>2</sup>University of Leeds, School of Earth and Environment, Leeds, U. K. E-mail: r.clark@see.leeds.ac.uk.

<sup>3</sup>University of Alberta, Department of Physics, Edmonton, Canada. E-mail: mirko.vanderbaan@ualberta.ca.

© 2012 Society of Exploration Geophysicists. All rights reserved.

The information that attenuation imparts to the seismic signal also can be a useful tool for reservoir characterization. By measuring attenuation, the reservoir properties that caused the amplitude losses may be inferred. For example: Attenuation in partially saturated media responds to changes in gas saturation (Winkler and Nur, 1982), which may help determine the contents of a reservoir; Attenuation is more sensitive than velocity to fracture azimuth (Clark et al., 2001; Maultzsch et al., 2007; Clark et al., 2009), and may be used as a mapping tool to target reservoir development; Injected steam causes changes in the mobility of reservoir fluids, and attenuation may be used to monitor these changes to optimize the injection process (Macrides and Kanasewich, 1987). Attenuation is therefore a desirable parameter to estimate with accuracy and precision.

A number of factors make the accurate determination of attenuation elusive. The primary difficulty comes from the effects on the seismic spectrum from interference of different seismic arrivals. The resulting spectral notching causes attenuation measurements to be highly bandwidth dependent, and also introduces bias into the results. Other complications arise from angle-dependent effects that hamper accurate interval measurements, and processing artifacts that change the spectrum of the wavelet. The QVO method (Dasgupta and Clark, 1998) seeks to improve the quality of attenuation measurements over those made from stacked data. By accounting for the differences in accumulated attenuation in each prestack trace, more accurate values can be achieved. Furthermore, prestack calculations avoid the spectral distortion in the wavelet caused by artifacts such as normal moveout (NMO) stretch or misaligned events, and prestack processes such as deconvolution, which make reliable values of attenuation difficult to quantify (Dasgupta and Clark, 1998; Ebrom, 2004). The effectiveness of QVO has been demonstrated in a number of applications, including discrimination of lithology types (Dasgupta and Clark, 1998; Hackert and Parra, 2004), azimuthal discrimination of fractures (Clark et al., 2009; Moffat et al., 2009), and time-lapse changes (Clark et al., 2001; Blanchard et al., 2009). Along with the successes however, the QVO method is also sensitive to corrupting influences such as spectral interference (Carter, 2003), source and receiver directivity (Hustedt and Clark, 1999), and attenuation anisotropy in the overburden.

In Part 1 of this paper, we introduce a robust method for measuring effective attenuation from surface seismic data. The prestack  $Q$ -inversion (PSQI) method that we demonstrate seeks to measure accurately the effective attenuation of an interval by minimizing factors that mask its true value. In Part 2 of this paper, we demonstrate the technique on a shallow 3D seismic survey, and compared the measurements to another  $Q$ -estimation technique, as well as measurements from a vertical seismic profile.

To minimize the effects of spectral interference in the calculations, spectra are calculated using a variable-window time-frequency transform (Reine et al., 2009). To reduce further the influence of these effects as well as noise, we introduce a scheme to invert for  $1/Q$  from natural log spectral-ratio data, simultaneously using all of the prestack data from a common midpoint (CMP) gather. While the inversion of natural log spectral-ratio data is often done with respect to frequency for a single fixed traveltime difference, this is not a requirement of the spectral-ratio method. This is demonstrated by Jeng et al. (1999), who invert the natural log spectral ratios for a fixed frequency over multiple traveltime differences. Finally, to address the problem of angle-dependent

effects, such as directivity, anisotropy, and raypath differences, we transform the data into the  $\tau$ - $p$  domain. For a medium with laterally homogeneous velocity and attenuation, this allows spectral ratios to be calculated for reflections on the same raypath in the overburden.

We begin by formulating the attenuation problem and discuss the complicating factors that must be addressed. We use a number of synthetic experiments to demonstrate how many of these problems can be eliminated through the use of the workflow components outlined above. In Part 2 of the paper (Reine et al., this issue), we demonstrate the PSQI method with an analysis of CMP data from a shallow 3D land-seismic survey, and show that the measured values are more stable than those obtained with the QVO method, and have reasonable magnitude when compared to vertical seismic profile (VSP) measurements.

## THEORY

The amplitude spectrum  $S(f)$  of a spherical wave traveling through a layered medium not only experiences exponential decay due to attenuation, but also includes amplitude losses due to energy partitioning  $P$  from reflection and transmission at impedance interfaces and geometric spreading  $G$ . If dispersion is neglected, these latter two terms are independent of frequency  $f$ . For an initial source amplitude spectrum  $S_0(f)$ , the spectrum of a given reflection can therefore be described by

$$S(f) = PG \cdot S_0(f) e^{-\frac{\pi f t}{Q_e}}, \quad (1)$$

where  $Q_e$  is the average effective quality factor over the travel path, related to attenuation  $\alpha$  by

$$\alpha = \frac{\pi f}{Q_e v} \quad (2)$$

(Aki and Richards, 2002). In equation 1, the path length and phase velocity  $v$  have been replaced with the elapsed traveltime  $t$ . The quantity  $Q_e$  is an effective value because it contains intrinsic effects  $Q_i$ , as well as apparent effects  $Q_a$ , such as those due to scattering. The three values are related by

$$\frac{1}{Q_e} = \frac{1}{Q_i} + \frac{1}{Q_a} \quad (3)$$

(Spencer et al., 1982).

### Spectral ratios

To measure  $1/Q$  between two reflections, the ratio of their two spectra  $S_1(f)$  and  $S_2(f)$ , may be taken, eliminating the need to know the source spectrum (Tonn, 1991). By taking the natural log of the spectral ratio, the function becomes a linear problem with respect to frequency or traveltime difference, allowing a range of linear inversion techniques to be applied to the measured data. This natural log spectral ratio is given by

$$\ln \left[ \frac{S_2(f)}{S_1(f)} \right] = -\frac{\pi}{Q} \Delta t f + \ln(PG), \quad (4)$$

where  $\Delta t$  is the traveltime difference between the two reflections, and  $Q$  refers to the effective quality factor for the interval. The terms  $P$  and  $G$  are simplified here to refer to the ratios between the two

reflections for the energy partitioning and geometric spreading terms, respectively. We have assumed in this relationship that the spectral behavior of the reflectivity is the same surrounding both events. If the spectral behavior is not the same and the reflectivity of the data is known confidently, it is possible to apply a correction to the measured spectrum to improve the attenuation estimate (Hackert and Parra, 2004).

Spectral measurements of the reflected wave are complicated by interference effects resulting from closely spaced events. Intrabed multiples and adjacent reflections cause the measured spectrum to exhibit peaks and notches, inhibiting the ability to measure intrinsic attenuation (Carter, 2003). To minimize these contributions, it is desirable to measure the spectrum using a variable-window time-frequency transform, such as the S-transform (Stockwell et al., 1996). Because there is less interference with the scattered coda and adjacent reflections, the use of a variable-window transform allows for more precise and accurate attenuation measurements (Reine et al., 2009).

If we wish to generalize equation 1 to refer to a reflection from a fixed interface for an arbitrary raypath, then several variables become dependent on the takeoff angle  $\theta$ . Traveltime  $t$  and energy partitioning  $P$  are clearly dependent on takeoff angle  $\theta$ , however  $1/Q$  may also have this dependency when it is anisotropic (Carcione and Cavallini, 1995; Zhu and Tsvankin, 2006). Because different takeoff angles are considered, the potential for a directionally dependent source or receiver array is also introduced, and the directivity term  $D^\theta(f)$  must be considered, leading to

$$S^\theta(f) = D^\theta(f)P^\theta G^\theta S_0(f)e^{-\frac{\pi f t}{Qc}}, \quad (5)$$

where the superscript  $\theta$  denotes an angle-dependency.

When considering arbitrary takeoff angles, the spectral-ratio between two events is more complex than presented in equation 4 (Figure 1a). If, for example, the amplitude spectra of two reflections with a common offset are compared, their takeoff angles and therefore raypaths will be different. This even includes the situation where a fixed-reference spectrum is used. Due to these arbitrary raypaths, the traveltimes and  $1/Q$  values within a single layer may differ for the two measurements. Along with the addition of the directivity terms, this results in a spectral-ratio relationship which is complicated, and nonlinear. To properly isolate the  $1/Q$  of a target layer, we consider the advantages of working in the  $\tau$ - $p$  domain.

**$\tau$ - $p$  domain**

By matching events with a constant horizontal slowness, Snell’s law ensures that these reflections occur along the same raypath in the overburden when laterally homogeneous velocity and attenuation are assumed. Using these matched reflections, it is no longer necessary to ignore the complications introduced by angular dependencies such as raypath length, attenuation anisotropy, and directivity. Instead, the angle-dependency of the reflection amplitudes may be canceled using the spectral-ratio of the coincident events (Carter, 2003; Behura and Tsvankin, 2009) (Figure 1b).

Reflections with constant horizontal slowness may be identified in the  $t$ - $x$  domain by matching the instantaneous time slopes of different reflections (Behura and Tsvankin, 2009). This method first requires an accurate determination of the reflection traveltimes.

Alternatively, we achieve the same matching by analyzing constant horizontal-slowness traces in the  $\tau$ - $p$  domain. One advantage of this approach is that the integration of amplitudes also makes the  $\tau$ - $p$  data less prone to static shifts and local noise; however, care must be exercised to avoid the introduction of transform artifacts.

The  $\tau$ - $p$  transform decomposes a prestack spherical-wave response  $s$  into its plane-wave components  $\tilde{s}$ , each defined by a horizontal slowness  $p$  (Brysk and McCowan, 1986). The term  $\tau$  refers to the vertical component of traveltime for the plane wave (Diebold and Stoffa, 1981), or its intercept time, defined by

$$\tau = t - px, \quad (6)$$

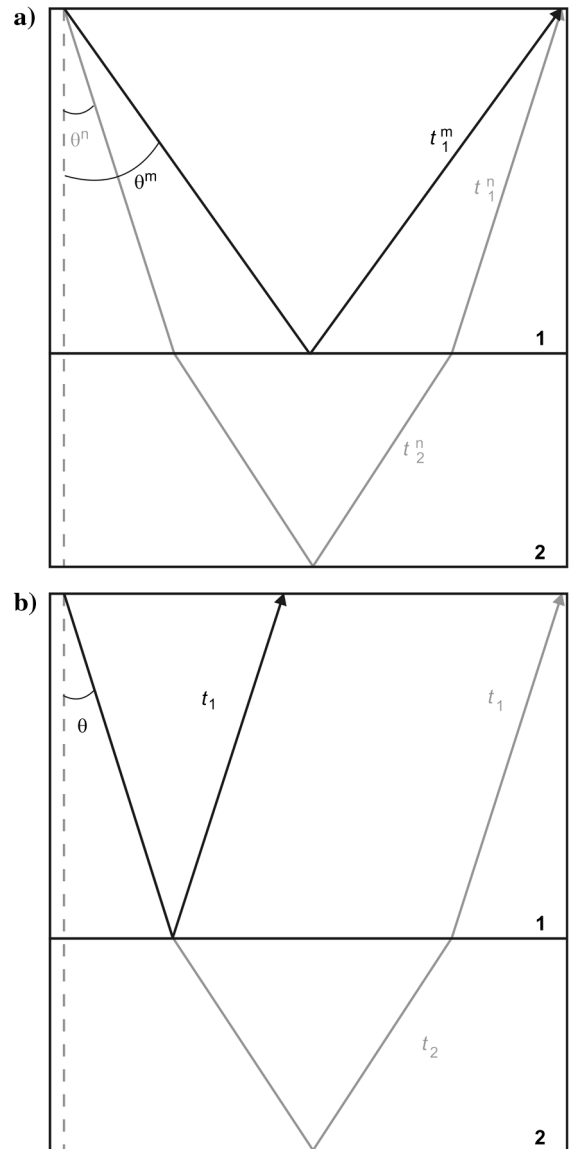


Figure 1. Raypaths of a reference (black) and measured (gray) reflection. (a) For arbitrary takeoff angles, including the case of common-offset reflections, the paths are different in the overburden. (b) When the horizontal slowness, and therefore takeoff angle, of the rays is the same, the overburden paths are the same.

where  $t$  is travelttime and  $x$  is the source-receiver offset. For a point source in 2D space, or a line-source in 3D, the  $\tau$ - $p$  transform is a simple slant stack, whose definition is

$$\tilde{s}(\tau, p) = \int_{-\infty}^{\infty} s(\tau + px, x) dx \quad (7)$$

(Chapman, 1981).

Although equation 7 is kinematically correct for a point source in 3D space, the amplitudes in this situation are not properly reconstructed, and the assumed plane-wave experiences geometric spreading in the out-of-plane coordinate (van der Baan, 2004). If these effects need to be accounted for, a 3D  $\tau$ - $p$  transform (Chapman, 1981; Brysk and McCowan, 1986) must be used, or a lateral filter to convert the amplitudes to their line-source equivalents (Wapenaar et al., 1992) must be applied prior to the 2D transform.

For the unflattened prestack gathers in the  $\tau$ - $p$  domain, knowledge of the reflection moveout behavior is necessary to track individual interfaces. The moveout of a reflection from the base of a homogeneous and isotropic layer follows an ellipse in the  $\tau$ - $p$  domain (Schultz and Claerbout, 1978). For layered media, the equivalent moveout curve is the sum of all interval moveouts down to the reflection. In anisotropic media with transverse isotropy, van der Baan and Kendall (2002) show that the  $\tau$ - $p$  domain moveout within a given layer  $\tau_i$  can be given by

$$\tau_i = \tau_{0i} \left( 1 - \frac{p^2 v_i^2}{1 - 2\eta_i p^2 v_i^2} \right)^{\frac{1}{2}}, \quad (8)$$

where  $\tau_{0i}$  is the interval travelttime for a vertical-incidence wave,  $v_i$  is the interval stacking velocity, and  $\eta_i$  is the associated anisotropy parameter defined by Alkhalifah and Tsvankin (1995). The total moveout for a multilayer geometry is given by the sum of the interval values

$$\tau = \sum \tau_i. \quad (9)$$

Whereas the  $\tau$ - $p$  moveout curves refer to the vertical travelttime component for plane waves, the full travelttime is needed for the inversion of  $1/Q$ . Based on the  $\tau$ - $p$  moveout relationship (equation 8) and the definition of  $\tau$  (equation 6) it follows that

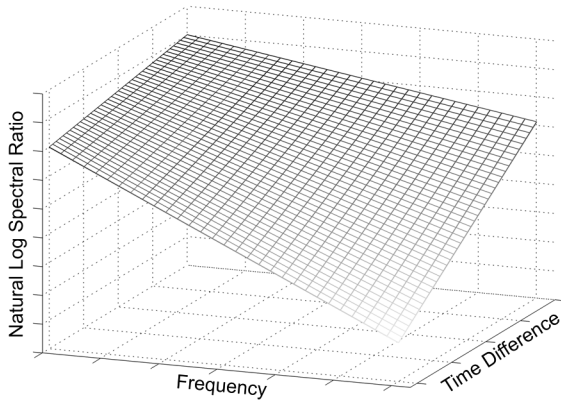


Figure 2. The natural log spectral ratios for multiple traces may be combined to form a smooth surface which decreases linearly in value as either frequency or travelttime difference increase.

$$\sum \frac{d}{dp} \tau_i = -x. \quad (10)$$

Applying this to equation 8 gives the equivalent offset for a point in  $\tau$ - $p$  space

$$x = \sum \frac{\tau_{0i} p v_i^2}{(1 - 2\eta_i p^2 v_i^2)^2 [1 - p^2 v_i^2 (1 - 2\eta_i p^2 v_i^2)^{-1}]^{\frac{1}{2}}}. \quad (11)$$

By solving the interval  $\tau$ - $p$  domain moveout (equation 8) for  $\tau_{0i}$ , and substituting into equation 11, the  $\tau$  definition given in equation 6 may again be employed to convert this equivalent offset to an equivalent travelttime

$$t = \tau + \sum \frac{\tau_i p^2 v_i^2}{(1 - 2\eta_i p^2 v_i^2)^2 [1 - p^2 v_i^2 (1 - 2\eta_i p^2 v_i^2)^{-1}]}. \quad (12)$$

Thus, for any point in  $\tau$ - $p$  space with a given  $\tau$  and  $p$ , equation 12 may be used to calculate the two-way travelttime, using the knowledge of the values  $v_i$  and  $\eta_i$  from velocity analysis, and  $\tau_i$  from equation 8. Interval velocity values are obtained from the effective measurements through Dix's equation or similar layer stripping procedures (van der Baan and Kendall, 2002; van der Baan, 2004).

### Inversion scheme

Once an appropriate choice of reference and measured spectra are made, group attenuation, in the form of  $1/Q$ , may be inverted from the natural log spectral ratio (equation 4). In a two-step inversion, such as that used in QVO (Dasgupta and Clark, 1998) the idea of a single-time inversion is extended for a prestack surface seismic gather. To determine the attenuation for the gather, the slope of the natural log spectral-ratio  $A$  is first determined for each offset trace

$$A = -\frac{\pi \Delta t}{Q}. \quad (13)$$

This is followed by a second inversion of the linear relationship between slopes  $A$  and travelttime-difference  $\Delta t$

$$A = A' \Delta t + B', \quad (14)$$

where

$$A' = -\frac{\pi}{Q}, \quad (15)$$

and  $B'$  is expected to be zero. This allows the determination of slope, and hence  $1/Q$  at zero-offset travelttime difference  $A(t_0)$ . By using multiple measurements of the same interval, the QVO method takes statistical advantage of the number of prestack traces.

We alter this approach to perform the inversion for  $1/Q$  in a single step. First, such that equation 4 is a linear equation in travelttime difference  $\Delta t$  and frequency  $f$ , we assume that the quality factor in the target layer is isotropic in the vertical plane as well as being homogeneous. This does not change the ability of the approach to deal with anisotropic attenuation in the overburden, which is addressed by operating in the  $\tau$ - $p$  domain. Furthermore, the energy partitioning and geometric spreading terms are assumed

to be independent of frequency, that is, the effects of dispersion and attenuation on reflectivity are ignored.

With these conditions, equation 4 describes a smoothly varying surface in  $\Delta t$  and  $f$  coordinates (Figure 2). As either coordinate increases in value, the natural log spectral ratio decreases. With either coordinate fixed, the natural log spectral ratio retains its linear behavior. Specifically for a fixed  $\Delta t$ , the typical situation of a single measurement is represented.

Analytically, this linear system of equations,  $\mathbf{d} = \mathbf{G}\mathbf{m}$ , may be expressed by

$$\begin{pmatrix} d_{11} \\ d_{21} \\ \vdots \\ d_{N1} \\ d_{12} \\ d_{22} \\ \vdots \\ d_{N2} \\ \vdots \\ d_{NM} \end{pmatrix} = \begin{pmatrix} \Delta t_1 f_1 & 1 & 0 & \dots & 0 \\ \Delta t_2 f_1 & 0 & 1 & \dots & 0 \\ \vdots & \vdots & \vdots & \ddots & \vdots \\ \Delta t_N f_1 & 0 & 0 & \dots & 1 \\ \Delta t_1 f_2 & 1 & 0 & \dots & 0 \\ \Delta t_2 f_2 & 0 & 1 & \dots & 0 \\ \vdots & \vdots & \vdots & \ddots & \vdots \\ \Delta t_N f_2 & 0 & 0 & \dots & 1 \\ \vdots & \vdots & \vdots & \ddots & \vdots \\ \Delta t_N f_M & 0 & 0 & \dots & 1 \end{pmatrix} \begin{pmatrix} A \\ B_1 \\ B_2 \\ \vdots \\ B_N \end{pmatrix}, \quad (16)$$

where the elements  $d_{nm}$  correspond to the natural log spectral-ratio measurement for traveltime-difference  $n$ , and frequency  $m$ . Here, the model parameters  $A$  and  $B_n$  are defined by

$$A = -\frac{\pi}{Q}, \quad (17)$$

and

$$B_n = \ln(P_n G_n). \quad (18)$$

The data in equation 16 have been ordered such that each fixed  $\Delta t$  is associated with a unique  $B_n$  in the model vector. This allows frequency-independent variability of the trace amplitudes due to elastic effects, without affecting the simultaneous determination of  $A$ . From equation 18, the absence of geometric spreading, such as the case where plane waves are considered, results in the  $B_n$  terms relating directly to the amplitude shift caused by angle-dependent reflection and transmission coefficients

$$P = \left| \frac{R_L}{R_1} \right| \prod_{i=1}^{L-1} \hat{T}_i \hat{f}_i. \quad (19)$$

Here,  $R_1$  and  $R_L$  are the reflection coefficients for the reference and measured reflections, respectively, and  $T_i$  is the transmission coefficient of interface  $i$  from the  $L$  layers separating the two events. Upgoing and downgoing coefficients are considered, as indicated by the annotations. For plane waves,  $R$  and  $T$  may be calculated using the Knott-Zoeppritz equations (Aki and Richards, 2002). This isolation of energy partitioning information is significant because the inversion not only produces information about  $1/Q$ , but also amplitude variation with angle (AVA) results. The change in amplitude with incidence angle has the advantage of being free from attenuation amplitude losses, although any reflectivity resulting purely from a  $1/Q$  contrast is still inherent in the results. This AVA information is especially useful if the reference reflectivity is known in advance, or the source spectrum is known. The

measurement of AVA in the  $\tau$ - $p$  domain is in many ways superior to  $t$ - $x$  domain measurements (van der Baan and Smit, 2006), which is another reason why it is a complimentary domain of operation for the PSQI method.

Equation 16 has a least-squares solution of

$$\mathbf{m} = (\mathbf{G}^T \mathbf{W} \mathbf{G})^{-1} \mathbf{G}^T \mathbf{W} \mathbf{d}, \quad (20)$$

where  $\mathbf{W}$  is the weighting matrix for the measured data (Menke, 1989). This weighting matrix may be defined in a number of different fashions. For a measurement at each frequency and traveltime difference, the weighting elements are the inverse of the data covariance matrix. Alternatively, the weighting function may be defined by the coherence function of the data (White, 1984), or in the case of time-lapse analysis, by inter-vintage cross-correlation coefficients (Blanchard et al., 2009). The function of the weighting matrix is to reduce the influence of unpredictable elements in the data. By allowing the weights to vary with frequency and traveltime difference, we reduce the influence of those components suspected to be more prone to noise.

Finally, the uncertainty in  $1/Q$  is found from the model covariance matrix, along with error propagation principles (Taylor, 1997). It should be noted that this treatment of error is valid for statistical fluctuations in the data; however it does not incorporate the systematic bias that is introduced by apparent attenuation effects.

## SYNTHETIC DATA

We first demonstrate how the choice of inversion scheme influences the measured attenuation in the presence of spectral interference. A two-step inversion is compared to the proposed simultaneous inversion. For this demonstration, a numerical simulation and a synthetic seismogram are used. We then demonstrate how the complications introduced into the spectral ratios by raypath differences are reduced by operating on a constant horizontal-slowness trace. To this end, we create a synthetic model with a directional source array and no intrinsic attenuation. We then show that by calculating the spectral ratios along a single horizontal-slowness trace, the apparent attenuation introduced by directivity is nullified. This contrasts the attenuation calculated using a fixed isotropic reference. By isolating the target in the  $\tau$ - $p$  domain, this source of error is removed from the spectral-ratio process. Finally, we illustrate the relationship between the inverted  $B_n$  parameters and the energy partitioning terms using a synthetic seismogram.

### Reduced spectral interference effects

#### Numerical simulation

We create a numerical surface representing equation 4, with input values of  $-\frac{\pi}{Q} = -10$  and a constant  $\ln(P_n G_n) = 10$ . The time difference varies from 0.0 s to 1.0 s, and the frequency ranges from 0 Hz to 100 Hz. We then consider two noisy variants of this surface simulating features which are commonly found in natural log spectral-ratio data (Figure 3). The first variant is a spike of amplitude 500, which is added to two points on the basic surface. This represents features caused by effects such as localized spectral notching or noise. The second case is the basic surface with the addition of a staircase trend of amplitude  $-500$ . The second irregularity

simulates an offset-dependent tuning effect, where the amplitude spectrum is notched at a different frequency for each trace.

The attenuation results from inverting the test surfaces with the two-step and simultaneous inversions with a constant weighting function are shown in Table 1. In both simulations, the simultaneous inversion is more accurate than the two-step approach in its determination of  $A = -\frac{\pi}{Q}$ . For the spiked surface, the inversion is more heavily influenced by the outliers, producing an  $A$  increase of 6.2% over the input value. The simultaneous inversion more closely follows the input data, with a smaller 1.4% increase in  $A$ . For

the staircase surface data, the influence of the irregularity on the two-step inversion is much greater. Because each trace is biased, the inversion of the individual slopes is also heavily affected (45% error). By constraining the model parameters in two coordinates, the simultaneous inversion significantly reduces the influence of the staircase, producing only a 1.7% error.

*Synthetic data*

For a more realistic demonstration of the ability of the simultaneous inversion scheme to reduce the influence of spectral notching,

**Table 1. The input  $A = -\frac{\pi}{Q}$  is compared to the value recovered by the two-step and simultaneous inversions. The simultaneous inversion reduces the effects of simulated spectral interference, and is therefore more attractive for attenuation analysis than the two-step approach.**

|           | Input A | Simultaneous A | 2-Step A |
|-----------|---------|----------------|----------|
| Spike     | -10     | -10.14         | -10.62   |
| Staircase | -10     | -9.83          | -14.55   |

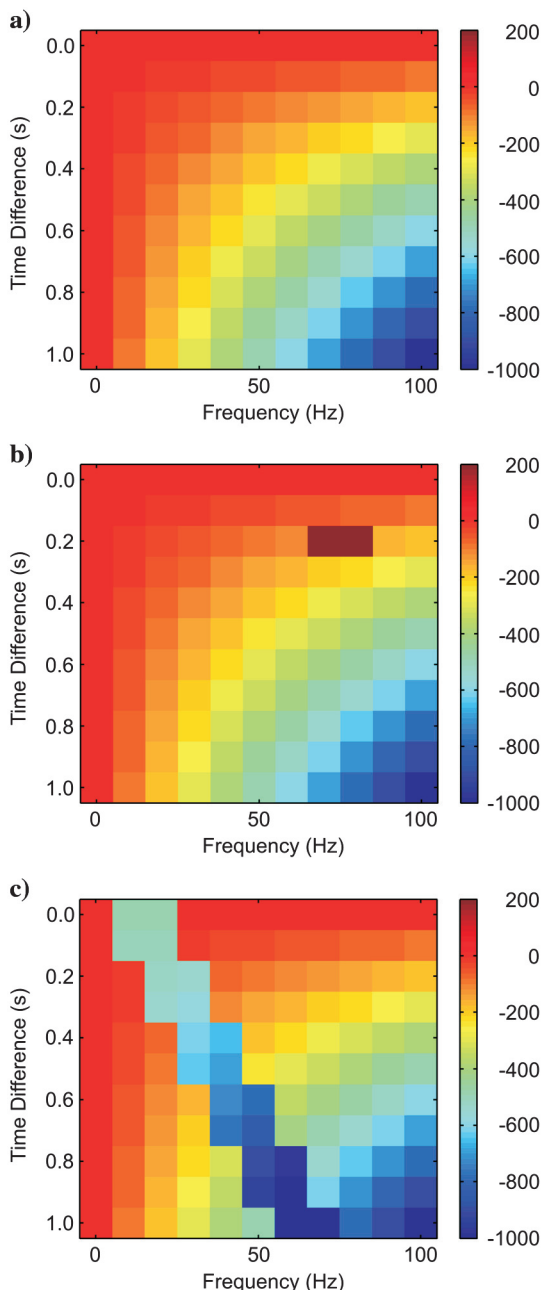


Figure 3. (a) The ideal natural log spectral ratio surface as described by equation 4. To test the inversion scheme, two variants of this surface are examined, simulating (b) localized spectral notching or noise, and (c) offset-dependent tuning.

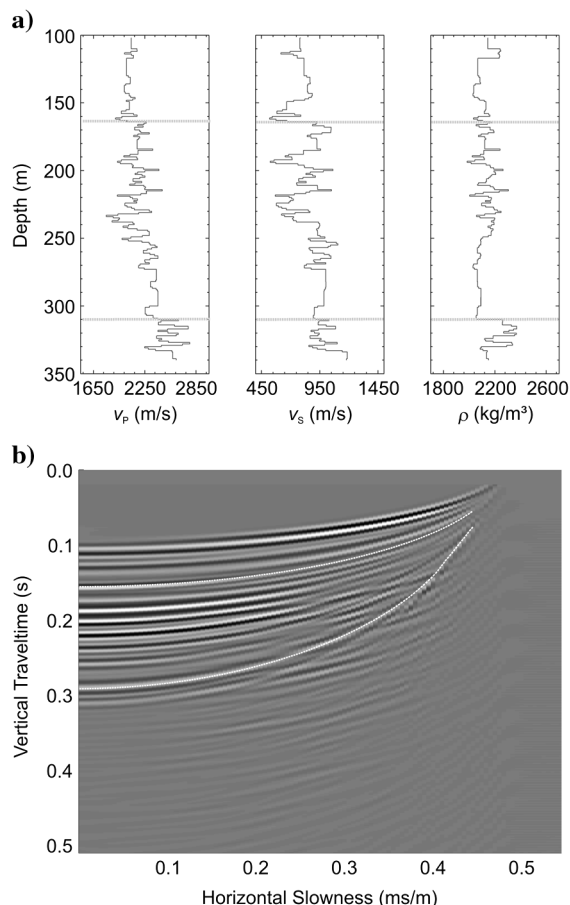


Figure 4. A blocked log model and its associated synthetic CMP gather in the  $\tau$ - $p$  domain. By using a thin-layered model, the presence of more realistic interference effects may be tested. The reference and measured reflections are indicated by dashed lines.

we measure the attenuation for a thin-layered synthetic CMP gather (Figure 4), using a variation on the synthetic test considered by (Reine et al., 2009). A blocked well-log model is used for input, and the synthetic data are generated in the  $\tau$ - $p$  domain using a reflectivity code (Kennett, 1983). The source is a zero-phase, 70 Hz Ricker wavelet, and 120 slownesses are calculated from  $0.5 \times 10^{-3}$  ms/m to 0.6 ms/m. A uniform constant- $Q$  intrinsic attenuation is used, with a value of  $1/Q_i = 0.02$ . Because of the effects of scattering, the effective attenuation is expected to be larger than the intrinsic input. Using wave localization theory (Shapiro and Zien, 1993; van der Baan, 2001), the model is assumed to have an exponential autocorrelation, leading to a maximum effective attenuation of approximately  $1/Q_e = 0.022$ .

The natural log spectral ratio is calculated between two major reflections with zero-slowness times of 156 ms and 292 ms using the short-time Fourier transform (STFT) with a window size of 101 ms. The STFT was specifically chosen so that there would be the most interference effects present (Reine et al., 2009). The slowness at which the lower event is refracted occurs near 0.4 ms/m, and we therefore only calculate the natural log spectral ratio out to this point. The natural log spectral-ratio surface is significantly affected by spectral notches which change position with offset (Figure 5). Because the result of the inversion is dependent on the bandwidth over which it is performed, we calculate  $1/Q$  for a range of bandwidths. The lower frequency of the bandwidth is varied from 0 Hz to 110 Hz and the upper frequency from 90 Hz to 220 Hz. A uniform weighting function is applied.

Figure 6 shows the results of the variable bandwidth calculations. In the ideal situation, this display would show a homogeneous  $1/Q_e = 0.022$  color for all possible bandwidth choices. The results of the simultaneous inversion show  $1/Q_e$  measurements which are much closer than the two-step inversion results to this expected effective attenuation. Within the bandwidth ranges shown in Figure 6, the median calculated values are  $1/Q_e = 0.021$  and  $1/Q_e = 0.032$  for the simultaneous and two-step approaches, respectively. The result of the simultaneous inversion therefore has a lower bias than the two-step inversion from the intrinsic  $1/Q$  and the effective  $1/Q$  of the model.

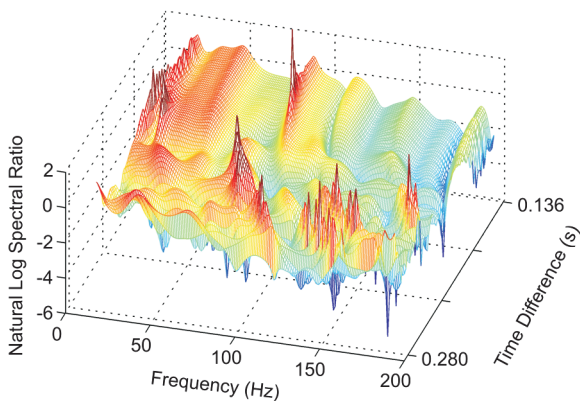


Figure 5. The natural log spectral ratio surface associated with the data shown in Figure 4. It is evident that the spectral interference notches and peaks change their frequency position with time difference.

### Directionally dependent effects

Directionally dependent effects such as directional source spectra, attenuation anisotropy, and travel path differences have the potential to distort the measured attenuation. Here, we simulate the directionally dependent amplitude response of a source or receiver system, whose apparent contribution to attenuation (Hustedt and Clark, 1999) is eliminated in the  $\tau$ - $p$  domain. We create a synthetic seismic CMP gather using a simple source array, whose amplitude response  $D(f)$  is given by the amplitude of the wavefield summed across each of the elements relative to the amplitude of the same elements located at the array center

$$D(f) = \left| \frac{\sin\left(n\pi\Delta x \frac{f \sin\theta}{v_0}\right)}{n \sin\left(\pi\Delta x \frac{f \sin\theta}{v_0}\right)} \right| \quad (21)$$

(Sheriff and Geldart, 1995). Here  $f$  is frequency,  $n$  is the number of elements in the array with spacing  $\Delta x$ ,  $\theta$  is the takeoff angle of the ray, and  $v_0$  is the velocity of the surrounding medium. We create a

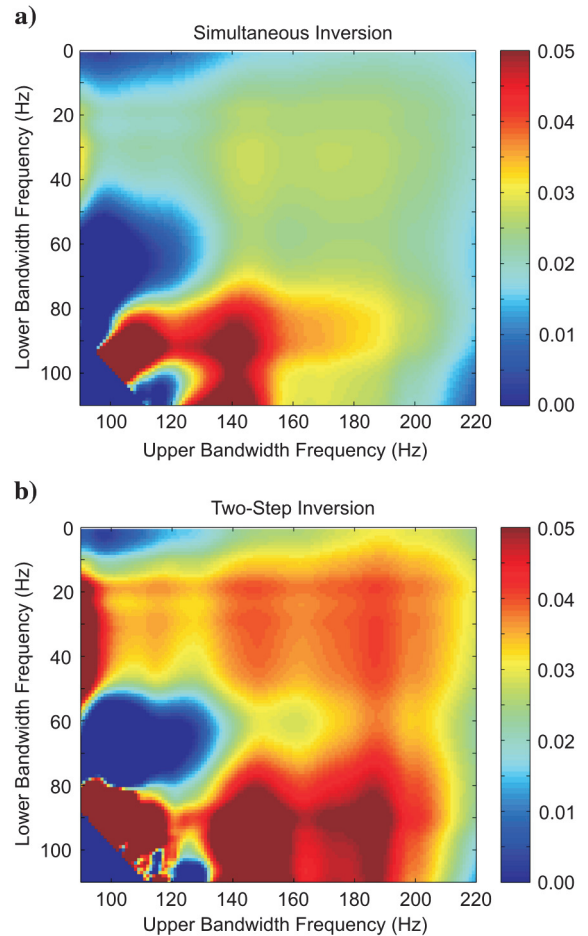


Figure 6.  $1/Q_e$  values (color) estimated for a range of bandwidths using the different inversion approaches. (a) The simultaneous inversion shows results which are more uniform, and with a median  $1/Q_e = 0.021$ , is much closer to the expected effective  $1/Q_e = 0.022$ , than (b) the two-step inversion with a median  $1/Q_e = 0.032$ .

five element array with an intraarray spacing of 5 m. The takeoff angles for each trace of the considered interface are determined by ray tracing the model. The amplitude response of this array for the synthetic data discussed below is shown in Figure 7.

A synthetic CMP is created in the  $t$ - $x$  domain using a reflectivity code with a 90°, 70 Hz Ricker source wavelet, and using the above array design. Offsets are calculated every 5 m from 0 m to 700 m corresponding to an offset to depth ratio up to two for the second interface. The synthetic data are then transformed into the  $\tau$ - $p$  domain (Figure 8). The input data are mirrored to reduce near-offset truncation artifacts from the  $\tau$ - $p$  transform. Five-hundred and one slownesses from  $-0.667$  ms/m to  $0.667$  ms/m are calculated, after which the negative slownesses are discarded.

The natural log spectral ratios are calculated for the array data in the  $t$ - $x$  and  $\tau$ - $p$  domains. A fixed-reference approach is taken for the  $t$ - $x$  data, in which an isotropic source function is assumed and used for the calculations at each offset. The zero-offset reflection from the first interface is used as this reference spectrum. In contrast, the reference event for the  $\tau$ - $p$  data is the reflection from the first interface on the same horizontal-slowness trace as the measured event. Because the model consists of coarse layers, the spectrum is locally stationary, and all spectral measurements are made using an STFT with a 101 ms window and a Hamming taper.

The natural log spectral-ratio surface for the  $t$ - $x$  data is shown in Figure 9a. Because there is no intrinsic attenuation in the model, no curvature is expected in the surface; however it is apparent from these data that this is not the case. The natural log spectral-ratio surface is effectively the natural log of the array amplitude response shown in Figure 7, because the input wavelet has been divided out. This produces a curvature in the natural log spectral-ratio surface which mimics intrinsic attenuation. The surface is inverted using a bandwidth of 20 Hz to 200 Hz, and the measured apparent attenuation has  $1/Q_e = 0.01$ , with negligible random uncertainty. This measurement bias is a significant amount of attenuation that cannot be ignored.

Conversely, the natural log spectral-ratio surface from the  $\tau$ - $p$  surface is much closer to the expected flat behavior (Figure 9b). There is a small ridge in the surface corresponding to the first notch in the array response. This notch causes a discontinuity in the

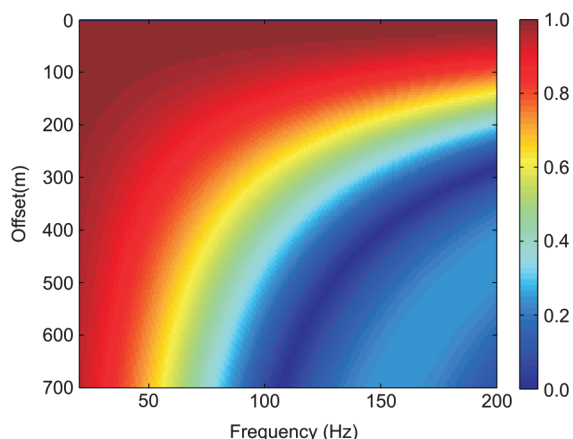


Figure 7. The amplitude response due to directivity effects depends on the offset considered as well as frequency. The response here corresponds to the amplitudes of the second interface of the synthetic model shown in Figure 8.

spectral division, resulting in numerical noise. There are also frequency-independent shifts in the surface due to the trace-to-trace energy partitioning term of the spectral-ratio equation. These shifts are accounted for in the inversion, resulting in a negligible measured apparent attenuation of  $1/Q_e = 0.00$ .

### Frequency-independent amplitudes

The  $B_n$  terms of the simultaneous inversion (equation 16) are directly related to the energy partitioning terms of equation 4. We refer to these as inversion intercepts, as they correspond to

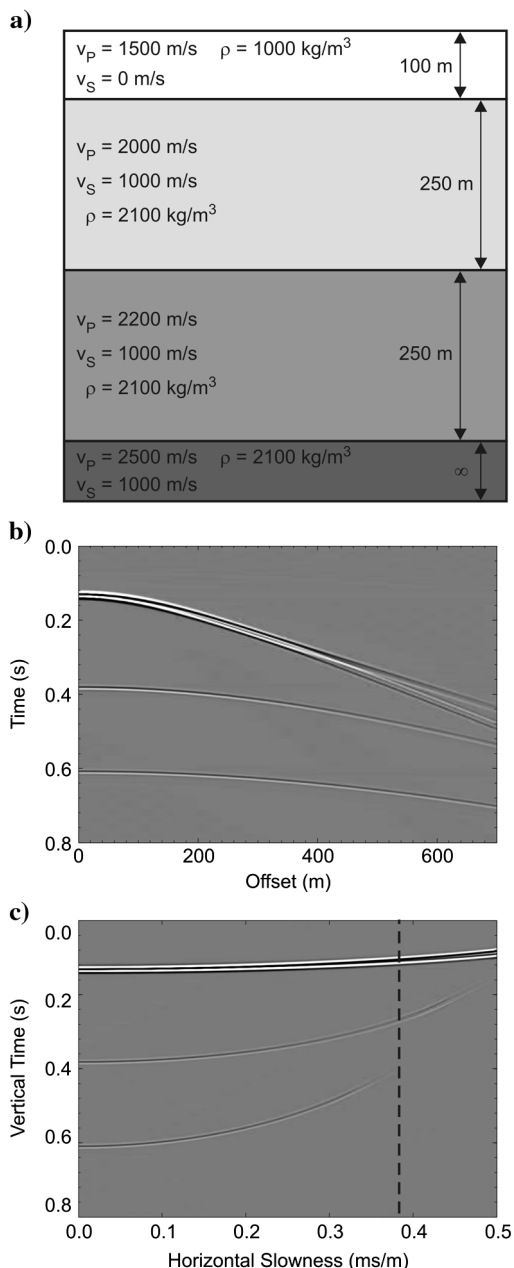


Figure 8. (a) A four-layer model and the associated synthetic CMP data in the (b)  $t$ - $x$  domain and (c) transformed into the  $\tau$ - $p$  domain. The vertical line on the  $\tau$ - $p$  data represents the horizontal slowness of the second reflection at the maximum recorded offset.

the intercepts of the natural log spectral-ratio solution for each discrete  $\Delta t$  at zero frequency. Synthetic data are modeled as plane waves directly in the  $\tau$ - $p$  domain (Kennett, 1983). We consider the three-layer model shown in Figure 10, where a pressure wave synthetic has been calculated over 200 slownesses, ranging from  $0.1 \times 10^{-3}$  ms/m to 0.5 ms/m, with a zero-phase, 70 Hz Ricker source wavelet. The natural log spectral-ratio surface experiences a shift over all frequencies for traces with mid to large time differences, corresponding to the near- and postcritical reflection coefficients at the interfaces.

We perform a simultaneous inversion of the natural log spectral-ratio data up to 0.314 ms/m using a constant weighting function. The attenuation measured has a value of  $1/Q = 0.019$ , which has only a 5% error from the input  $1/Q = 0.020$ . Figure 11 shows the inversion intercepts and the calculated energy partitioning term using the Knott-Zoeppritz equations. To account for residual geometric spreading, the two curves have been regularized such that they both start at the same value. There is excellent agreement between the two, confirming the relationship between the inversion intercept and the energy partitioning information.

For the more complicated synthetic considered previously (Figure 4), the intercept terms begin to deviate from the expected behavior governed by the energy partitioning equations. The experimental parameters are the same as those used in the previous use of this synthetic. As with conventional AVA analysis, this deviation is

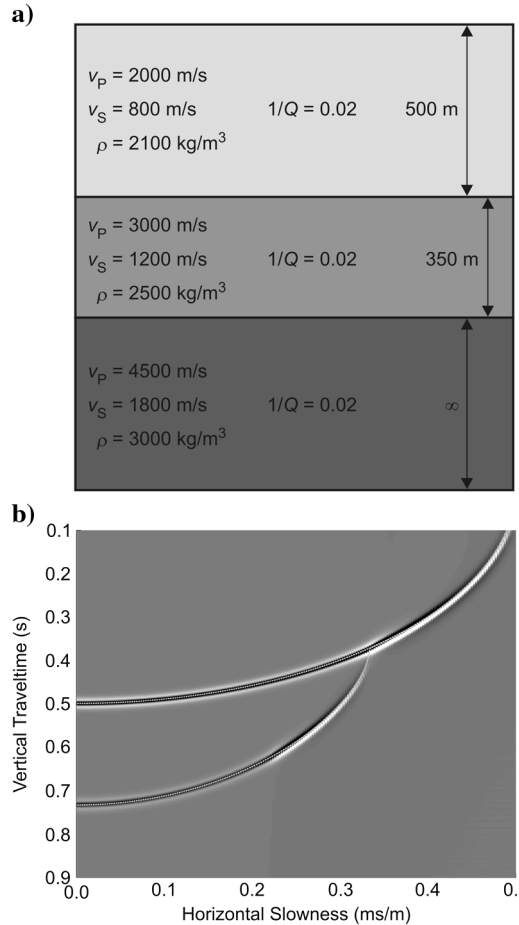


Figure 10. (a) A simple model and (b) the associated synthetic CMP data in the  $\tau$ - $p$  domain used to analyze the relationship between the inversion intercepts and energy partitioning terms. A coarse model is used so that the trace-to-trace amplitudes are not influenced by interference effects.

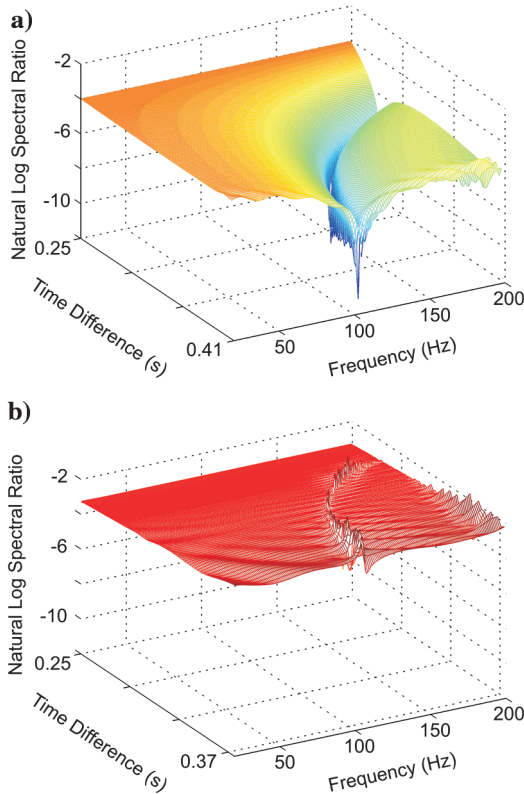


Figure 9. (a) The natural log spectral ratio surface for the fixed-reference,  $t$ - $x$  data. Although there is no intrinsic attenuation present, the presence of directivity introduces curvature, which mimics attenuation. (b) The same surface from the constant-slowness,  $\tau$ - $p$  data. There is no apparent curvature, and negligible apparent attenuation can be detected.

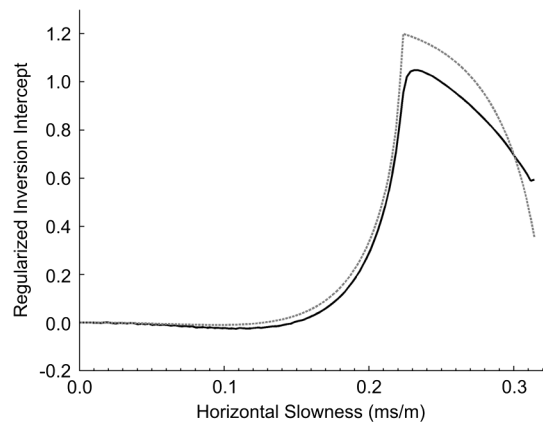


Figure 11. The calculated inversion intercepts (solid) and the natural log of the theoretical energy partitioning terms (dashed) regularized to start at the same value. There is excellent agreement between the two curves, confirming that energy partitioning information is recoverable through the inversion process.

caused by amplitude variations along the reflection due to interference effects. Because the amount of interference varies depending on the trace considered, the shift from the theoretical curve is not uniform. We calculate the expected  $P$  term from the input model, and compare this with the inversion intercept results. Figure 12 shows these two curves, which have been regularized to start at the same point. While there are fluctuations of the measured data about the theoretical curve, there is also strong agreement between the two, demonstrating the potential to integrate amplitude and attenuation analyses using the proposed simultaneous inversion scheme.

## DISCUSSION

The natural log spectral-ratio surface for a CMP gather contains information about the attenuation between the two interfaces considered. While the data are expected to lie on a smoothly varying surface described by equation 4, in practice there are significant deviations from this surface due to interference effects and noise. To extract the attenuation information from the data properly, it is necessary to use an inversion approach that is not severely affected by these deviations.

An inverse problem which treats the coordinates of frequency and time difference simultaneously, rather than in two steps, is much less affected by arbitrary spikes and ridges in the data. This is because the same model parameters are used to constrain the solution in the frequency and time difference coordinates, both of which are expected to obey linear behavior. Additionally, by allowing the intercept term of the inversion to vary from trace-to-trace, frequency-independent amplitudes do not affect the measurement of attenuation. Random noise causes variability in the data, and calculating an appropriate weighting function for the inversion further reduces its effects. By using our proposed inversion scheme (equation 16, attenuation in the presence of scattering, tuning effects, and noise may be more closely recovered.

Although a least-squares approach has been used for the inversion examples here, this is not a requirement of the simultaneous inversion. In fact, in the presence of spectral interference, this might not be an appropriate model (Reine, 2009). Alternative methods,

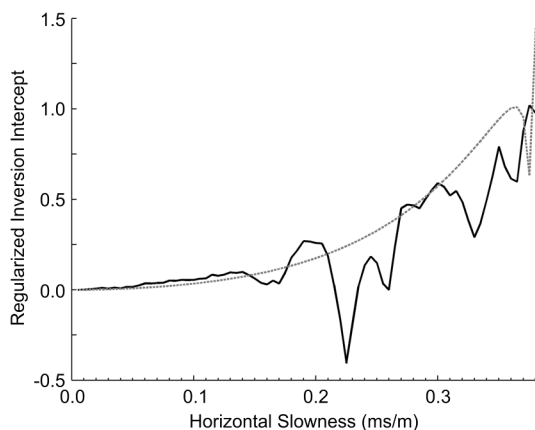


Figure 12. A comparison of the inversion intercept terms (solid) and the natural log of the energy partitioning terms (dashed) for the blocked log model shown in Figure 4. The curves have been regularized to start at the same value. Although there are fluctuations in the measured data, overall there is good agreement between the two curves.

such as an iterative reweighted least-squares inversion (Gubbins, 2004), may be used to allow for an adaptive,  $L_p$ -norm solution.

One of the advantages of the spectral-ratio method is that there are no assumptions about the analytical nature of the spectrum, allowing for a flexible parameterization of the inversion. Although we assume a frequency-independent  $1/Q$ , it is not a requirement of the method. Reid et al. (2001), for example, allow for a power-law relationship between attenuation and frequency, performing a non-linear inversion of the spectral-ratio data to obtain the power explicitly along with  $1/Q$ . Such frequency behavior could also be incorporated into the proposed inversion scheme. Because of the strong indication from laboratory studies that  $1/Q$  is frequency dependent, it is prudent to use a method, such as the spectral-ratio, which can accommodate linearized relationships with a frequency-dependent  $1/Q$ .

As presented, we have sacrificed the ability to measure attenuation variability or anisotropy in the target layer to achieve more robust attenuation measurements. This was done through the assumption of an isotropic and homogeneous target layer. If strong attenuation variation with angle is expected, an adjustment to the inversion scheme or data sectoring is necessary.

To evaluate an anisotropic target layer, an analytical form of  $Q$ -anisotropy such as that given by Zhu and Tsvankin (2006) could possibly be used to redefine the model parameters of the inversion, such that an anisotropic attenuation may be obtained. Alternatively, it would also be possible to apply the same PSQI inversion incorporating different sectors of data. For azimuthally variable media, the CMP gather may be sectorized by azimuth prior to the  $\tau$ - $p$  transform, and each transformed sector analyzed individually. For a target with a vertical symmetry axis, the  $\tau$ - $p$  transformed data may be sectorized by horizontal slowness. While sectoring allows a smaller division of azimuths or incidence angles by relaxing the assumption of an isotropic target layer, some of the advantage of the simultaneous inversion is lost. Because spectral interference effects change frequency position with the different traveltimes differences considered, a reduction in the number of traces reduces the statistical ability of the inversion to overcome these effects, reducing to the extreme case in which each trace is treated individually.

In addition to attenuation, the simultaneous inversion scheme involves separate model parameters that contain information about the energy partitioning properties of the subsurface interfaces. In the absence of geometric spreading, this energy partitioning can be predicted using reflection and transmission coefficient data, shown in equation 19. From these inverted parameters, the potential exists to extract AVA information that is independent from the amplitude losses from attenuation, reducing a source of error in conventional AVA analysis (Luh, 1993). The problem becomes one of separating the AVA response of the measured and reference events. If the source spectrum is known and used as the reference, this separation is not important, as the inverted parameters give the effective AVA curve for the measured interface.

By mapping data recorded in the  $t$ - $x$  domain to traces corresponding to a constant ray parameter using the  $\tau$ - $p$  transform (equation 7), data may be analyzed along a constant horizontal-slowness trace, simplifying the natural log spectral-ratio equation. In the case where a directional source or receiver array was used, the use of a fixed reference spectrum introduced differential notching compared to the measured event. This results in a large amount of apparent attenuation. By operating along constant horizontal-slowness traces, the

notching is in the same location for both spectra, and the effects of the directivity cancel out upon division.

The  $\tau$ - $p$  transform as well as the horizontal-slowness matching in the  $t$ - $x$  domain (Behura and Tsvankin, 2009) allow for the interval, rather than a composite,  $1/Q$  to be obtained directly. This eliminates sources of error in the attenuation measurement due to properties of the CMP gather which change with incidence angle. The advantages of the  $\tau$ - $p$  transform are that the traveltimes of reflections need not be calculated in advance, and that there is a reduction in the random noise due to the slant-stack process. The cost of these advantages is the need to be vigilant in the choice of transform parameters to prevent the introduction of artifacts caused by aliasing and truncation. Aliasing requires that the slownesses calculated are appropriate for the density of acquired data. The use of a 2D  $\tau$ - $p$  transform and its assumption of azimuthal symmetry helps to reduce this spatial sampling requirement (Chapman, 1981; Brysk and McCowan, 1986), and steps can then be taken to properly account for 3D amplitudes (van der Baan, 2004). Truncation artifacts, caused by transforming data with a finite spread length, may be reduced by mirroring the data at near offsets, and by applying a taper function to the data at far offsets (Wang and Houseman, 1997). The data must be analyzed to see if these remaining artifacts pose a significant problem. Furthermore, when using large horizontal slownesses, it is important to truncate the data before the horizontal slowness of refraction or before the horizontal slownesses corresponding to the end of the  $t$ - $x$  offset range. Beyond these traces the data has an incomplete representation, and may produce inappropriate attenuation measurements.

## CONCLUSIONS

Because of spectral interference, accurate measurements of seismic attenuation can be difficult. By using prestack CMP gathers, the multitude of data allows the inverse problem to be better constrained. We have introduced an inversion scheme that solves for attenuation using all of the prestack traces simultaneously, by accounting for the linear dependence of the natural log spectral ratio on frequency and traveltime difference between a reference and measured reflection.

The proposed PSQI method is designed to provide a number of benefits to improve  $1/Q$  measurements. The simultaneous inversion significantly reduces the error in the attenuation measurement, as demonstrated by a simple numerical example and the expanded case of a thin-layered synthetic data set. The simultaneous inversion better recovers the input intrinsic attenuation in the model in the presence of scattering and tuning effects. An additional benefit of the inversion scheme is that the intercept terms relate directly to the energy partitioning of the measured reflection when geometrical spreading effects are eliminated. When the trace-dependent reflectivity of the reference event is known, the reflectivity of the measured reflection is also recovered, free from the effects of attenuation.

To optimize the performance of the simultaneous inversion, two additional components are employed for seismic attenuation measurement. First, as demonstrated in previous work, a variable-window time-frequency transform is used to minimize the spectral interference effects caused by closely spaced events. Second, a reference and measured event which share a constant ray parameter are identified. This is achieved with the  $\tau$ - $p$  transform, and allows the simplification of the calculations to meet the necessary assump-

tions in the inversion. This approach also allows angle-dependent overburden properties, such as source or receiver directivity or attenuation anisotropy, to cancel, isolating the target layer. While the inversion scheme does not require the use of variable-window spectral estimates, and could be applied to data in the  $t$ - $x$  domain, these components of the method are all designed to simplify the assumptions and optimize the inversion results. The end result is that by using all of the PSQI components together, the accuracy of the attenuation estimate is greatly improved.

## ACKNOWLEDGMENTS

This work was carried out as part of a Ph.D. project at the University of Leeds. We would like to thank Nexen Inc. for providing the funding for this research, as well as the well-log data in conjunction with OPTI Canada Inc. Processing software was provided by Landmark Graphics Corporation through the Landmark University Grant Program. Additionally, we thank Andy Carter for his assistance with the seismic reflectivity modelling code and his continued interest and feedback, as well as Yaping Zhu and an anonymous reviewer for their helpful comments.

## REFERENCES

- Aki, K., and P. G. Richards, 2002, *Quantitative seismology*, 2nd ed.: University Science Books.
- Alkhalifah, T., and I. Tsvankin, 1995, Velocity analysis for transversely isotropic media: *Geophysics*, **60**, 1550–1566, doi: [10.1190/1.1443888](https://doi.org/10.1190/1.1443888).
- Bansal, R., V. Khare, T. Jenkinson, M. Matheney, and A. Martinez, 2009, Correction for NMO stretch and differential attenuation in converted-wave data: A key enabling technology for prestack joint inversion of PP and PS data: *The Leading Edge*, **28**, 1182–1190, doi: [10.1190/1.3249772](https://doi.org/10.1190/1.3249772).
- Behura, J., and I. Tsvankin, 2009, Estimation of interval anisotropic attenuation from reflection data: *Geophysics*, **74**, no. 6, A69–A74, doi: [10.1190/1.3191733](https://doi.org/10.1190/1.3191733).
- Blanchard, T. D., R. A. Clark, and M. van der Baan, 2009, Monitoring pore fluid changes using time-lapse attenuation: *Research Workshop 2009, EAGE/SEG, Expanded Abstracts*, B03.
- Brysk, H., and D. W. McCowan, 1986, A slant-stack procedure for point-source data: *Geophysics*, **51**, 1370–1386, doi: [10.1190/1.1442187](https://doi.org/10.1190/1.1442187).
- Carcione, J. M., and F. Cavallini, 1995, Forbidden directions for inhomogeneous pure shear waves in dissipative anisotropic media: *Geophysics*, **60**, 522–530, doi: [10.1190/1.1443789](https://doi.org/10.1190/1.1443789).
- Carter, A. J., 2003, *Seismic wave attenuation from surface seismic reflection surveys — an exploration tool?*: Ph.D. thesis, University of Leeds.
- Causse, E., R. Mittet, and B. Ursin, 1999, Preconditioning of full-waveform inversion in viscoacoustic media: *Geophysics*, **64**, 130–145, doi: [10.1190/1.1444510](https://doi.org/10.1190/1.1444510).
- Chapman, C. H., 1981, Generalized radon transforms and slant stacks: *Geophysical Journal of the Royal Astronomical Society*, **66**, 445–453.
- Clark, R. A., P. M. Benson, A. J. Carter, and C. A. Guerrero Moreno, 2009, Anisotropic P-wave attenuation measured from a multi-azimuth surface seismic reflection survey: *Geophysical Prospecting*, **57**, 835–845, doi: [10.1111/gpr.2009.57.issue-5](https://doi.org/10.1111/gpr.2009.57.issue-5).
- Clark, R. A., A. J. Carter, P. C. Nevill, and P. M. Benson, 2001, Attenuation measurements from surface seismic data — Azimuthal variation and time-lapse case studies: 63rd Annual International Conference and Exhibition, EAGE, Expanded Abstracts, L-28.
- Dasgupta, R., and R. A. Clark, 1998, Estimation of Q from surface seismic reflection data: *Geophysics*, **63**, 2120–2128, doi: [10.1190/1.1444505](https://doi.org/10.1190/1.1444505).
- Diebold, J. B., and P. L. Stoffa, 1981, The traveltime equation, tau-p mapping, and inversion of common midpoint data: *Geophysics*, **46**, 238–254, doi: [10.1190/1.1441196](https://doi.org/10.1190/1.1441196).
- Dvorkin, J., and A. Nur, 1993, Dynamic poroelasticity: A unified model with the squirt and the biot mechanisms: *Geophysics*, **58**, 524–533, doi: [10.1190/1.1443435](https://doi.org/10.1190/1.1443435).
- Ebrom, D., 2004, The low-frequency gas shadow on seismic sections: *The Leading Edge*, **23**, 772, doi: [10.1190/1.1786898](https://doi.org/10.1190/1.1786898).
- Gubbins, D., 2004, *Time series analysis and inverse theory for geophysicists*: Cambridge University Press.

- Hackert, C. L., and J. O. Parra, 2004, Improving Q estimates from seismic reflection data using well-log-based localized spectral correction: *Geophysics*, **69**, 1521–1529, doi: [10.1190/1.1836825](https://doi.org/10.1190/1.1836825).
- Hustedt, B., and R. A. Clark, 1999, Source/receiver array directivity effects on marine seismic attenuation measurements: *Geophysical Prospecting*, **47**, 1105–1119, doi: [10.1046/j.1365-2478.1999.00169.x](https://doi.org/10.1046/j.1365-2478.1999.00169.x).
- Jeng, Y., J.-Y. Tsai, and S.-H. Chen, 1999, An improved method of determining near-surface Q: *Geophysics*, **64**, 1608–1617, doi: [10.1190/1.1444665](https://doi.org/10.1190/1.1444665).
- Johnston, D. H., M. N. Toksöz, and A. Timur, 1979, Attenuation of seismic waves in dry and saturated rocks: II. Mechanisms: *Geophysics*, **44**, 691–711, doi: [10.1190/1.1440970](https://doi.org/10.1190/1.1440970).
- Kaderali, A., M. Jones, and J. Howlett, 2007, White Rose seismic with well data constraints: A case history: *The Leading Edge*, **26**, 742–754, doi: [10.1190/1.2748491](https://doi.org/10.1190/1.2748491).
- Kennett, B. L. N., 1983, *Seismic wave propagation in stratified media*: Cambridge University Press.
- Luh, P. C., 1993, Wavelet attenuation and bright-spot detection, in J. P. Castagna, and M. M. Backus, eds., *Offset-dependent reflectivity: Theory and practice of AVO analysis: Investigations in geophysics*, **8**, 190–198.
- Macrides, C. G., and E. R. Kanasewich, 1987, Seismic attenuation and Poisson's ratios in oil sands from crosshole measurements: *Journal of the Canadian Society of Exploration Geophysicists*, **23**, 46–55.
- Maultzsch, S., M. Chapman, E. Liu, and X.-Y. Li, 2007, Modelling and analysis of attenuation anisotropy in multi-azimuth VSP data from the clair field: *Geophysical Prospecting*, **55**, 627–642, doi: [10.1111/gpr.2007.55.issue-5](https://doi.org/10.1111/gpr.2007.55.issue-5).
- Menke, W., 1989, *Geophysical data analysis: Discrete inverse theory*, Revised ed.: Academic Press Inc.
- Moffat, L. C., R. A. Clark, M. van der Baan, and T. Manning, 2009, Azimuthal variations of attenuation analysis applied on a 3D multi-azimuth towed-streamer dataset: *Research Workshop 2009, EAGE/SEG, Expanded Abstracts*, B06.
- Reid, F. J. L., P. H. Nguyen, C. MacBeth, R. A. Clark, and I. Magnus, 2001, Q estimates from North sea VSPs: 71st Annual Meeting, SEG, Expanded Abstracts, 440–443.
- Reine, C., 2009, *A robust prestack Q-inversion in the  $\tau$ -p domain using variable window spectral estimates*: PhD thesis University of Leeds.
- Reine, C., M. van der Baan, and R. Clark, 2009, The robustness of seismic attenuation measurements using fixed- and variable-window time-frequency transforms: *Geophysics*, **74**, no. 2, WA123–WA135, doi: [10.1190/1.3043726](https://doi.org/10.1190/1.3043726).
- Schultz, P. S., and J. F. Claerbout, 1978, Velocity estimation and downward continuation by wavefront synthesis: *Geophysics*, **43**, 691–714, doi: [10.1190/1.1440847](https://doi.org/10.1190/1.1440847).
- Shapiro, S. A., and H. Zien, 1993, The O'Doherty-Anstey formula and localization of seismic waves: *Geophysics*, **58**, 736–740, doi: [10.1190/1.1443458](https://doi.org/10.1190/1.1443458).
- Sheriff, R. E., and L. P. Geldart, 1995, *Exploration seismology*, 2nd ed.: Cambridge University Press.
- Spencer, T. W., J. R. Sonnad, and T. M. Butler, 1982, Seismic Q-Stratigraphy or dissipation: *Geophysics*, **47**, 16–24, doi: [10.1190/1.1441275](https://doi.org/10.1190/1.1441275).
- Stockwell, R. G., L. Mansinha, and R. P. Lowe, 1996, Localization of the complex spectrum: The S transform: *IEEE Transactions on Signal Processing*, **44**, 998–1001, doi: [10.1109/78.492555](https://doi.org/10.1109/78.492555).
- Taylor, J. R., 1997, *An introduction to error analysis: The study of uncertainties in physical measurements*, 2nd ed.: University Science Books.
- Tonn, R., 1991, The determination of the seismic quality factor Q from VSP data: A comparison of different computational methods: *Geophysical Prospecting*, **39**, 1–27, doi: [10.1111/gpr.1991.39.issue-1](https://doi.org/10.1111/gpr.1991.39.issue-1).
- van der Baan, M., 2001, Acoustic wave propagation in one-dimensional random media: The wave localization approach: *Geophysical Journal International*, **145**, 631–646, doi: [10.1046/j.1365-246x.2001.01405.x](https://doi.org/10.1046/j.1365-246x.2001.01405.x).
- van der Baan, M., 2004, Processing of anisotropic data in the  $\tau$ -p domain: I — Geometric spreading and moveout corrections: *Geophysics*, **69**, 719–730, doi: [10.1190/1.1759458](https://doi.org/10.1190/1.1759458).
- van der Baan, M., and J. M. Kendall, 2002, Estimating anisotropy parameters and traveltimes in the  $\tau$ -p domain: *Geophysics*, **67**, 1076–1086, doi: [10.1190/1.1500368](https://doi.org/10.1190/1.1500368).
- van der Baan, M., and D. Smit, 2006, Amplitude analysis of isotropic p-wave reflections: *Geophysics*, **71**, no. 6, C93–C103, doi: [10.1190/1.2335877](https://doi.org/10.1190/1.2335877).
- Wang, Y., 2002, A stable and efficient approach of inverse Q filtering: *Geophysics*, **67**, 657–663, doi: [10.1190/1.1468627](https://doi.org/10.1190/1.1468627).
- Wang, Y., and G. A. Houseman, 1997, Point-source  $\tau$ -p transform: A review and comparison of computational methods: *Geophysics*, **62**, 325–335, doi: [10.1190/1.1444134](https://doi.org/10.1190/1.1444134).
- Wapenaar, C. P. A., D. J. Verschuur, and P. Herrmann, 1992, Amplitude preprocessing of single and multicomponent seismic data: *Geophysics*, **57**, 1178–1188, doi: [10.1190/1.1443331](https://doi.org/10.1190/1.1443331).
- White, R. E., 1984, Signal and noise estimation from seismic reflection data using spectral coherence methods: *Proceedings of the IEEE*, **72**, 1340–1356, doi: [10.1109/PROC.1984.13022](https://doi.org/10.1109/PROC.1984.13022).
- Winkler, K. W., and A. Nur, 1982, Seismic attenuation: Effects of pore fluids and frictional sliding: *Geophysics*, **47**, 1–15, doi: [10.1190/1.1441276](https://doi.org/10.1190/1.1441276).
- Zhu, Y., and I. Tsvankin, 2006, Plane-wave propagation in attenuative transversely isotropic media: *Geophysics*, **71**, no. 2, T17–T30, doi: [10.1190/1.2187792](https://doi.org/10.1190/1.2187792).